ACS APPLIED MATERIALS & INTERFACES

Research Article

www.acsami.org

Enhanced Photocatalytic Activity in Electrospun Bismuth Vanadate Nanofibers with Phase Junction

Jing Cheng,[†] Jing Feng,[‡] and Wei Pan*[,†]

[†]State Key Laboratory of New Ceramics and Fine Processing, School of Materials Science and Engineering, Tsinghua University, Beijing 100084, People's Republic of China

[‡]School of Engineering and Applied Sciences, Harvard University, Cambridge, Massachusetts 02138, United States

Supporting Information

ABSTRACT: $BiVO_4$ nanofibers were successfully prepared by electrospinning and precisely controlled heat treatment. The obtained $BiVO_4$ nanofibers showed an enhanced photocatalytic activity in the degradation of rhodamine-B under visible light irradiation. The as-prepared nanofibers were characterized by means of numerous techniques. The enhanced photocatalyst activity is attributed to the formation of a phase junction of tetragonal sheelite (s-t) and monoclinic sheelite (s-m) phases in the electrospun $BiVO_4$ nanofibers. We have also investigated the band structure of $BiVO_4$ using first principle calculation. The main photon transition mechanism of the photocatalyst should be from the O 2p to V 3d state of s-m/t $BiVO_4$ nanofibers.

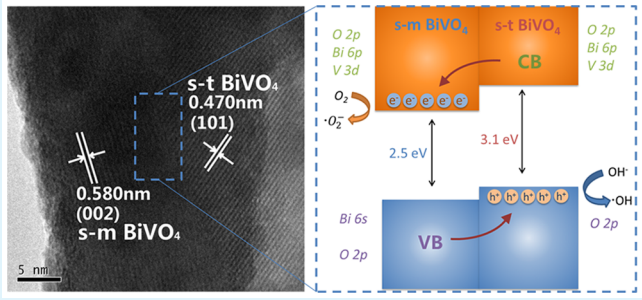

KEYWORDS: *$BiVO_4$, electrospinning, phase junction, photon absorption, first principle calculation*

INTRODUCTION

Nowadays, environment pollution is one of the most urgent issues facing modern society. As a result, photocatalysis has received extensive attention for water treatment, pollutant removal, and so on.[1] Because of the low cost and high efficiency, titanium dioxide is the most widely used photocatalyst at present.[2] However, TiO_2 can be activated only under UV radiation due to its limited band gap (E_g). Much research has been carried out on surface modification or doping to eliminate this drawback,[3−5] but there are still some problems. For example, the dopants usually act as recombination centers of the photogenerated electrons and holes, which is not conducive to the photocatalytic efficiency.[6] Therefore, a lot of effort has been focused on the design and development of nontitania-based semiconductor photocatalysts with visible light response, such as $BiVO_4$,[7] Bi_2WO_6,[8] $AgNbO_3$,[9] etc. These photocatalysts have been developed through band gap engineering; a continuous valence band is formed with Bi (6s), and V (3d) besides O (2p) orbital, which results in a decrease of the band gap.[10]

Among the various nontitania-based visible light-driven photocatalysts, $BiVO_4$ has been investigated during the past three decades because of its potential applications in many fields. $BiVO_4$ exhibits promising photocatalytic activity in water splitting and degradation of organic pollutants.[11,12] $BiVO_4$ also shows ferroelastic property[13] and ionic conductivity.[14] $BiVO_4$ exists in three different phases, tetragonal zircon (t-z), tetragonal sheelite (s-t), and monoclinic sheelite (s-m) structure.[15] The photocatalytic performance of $BiVO_4$ is strongly related to its crystal phase. It has been reported that the photocatalytic activity of the monoclinic $BiVO_4$ is much higher than those of the other two.[16] Yet it is still unclear whether the monoclinic $BiVO_4$ shows the best visible light-driven photcatalytic activity or the performance can be proved better with a mixture of tetragonal sheelite phase. Actually, it is known that the photocatalytic efficiency is mainly related to the specific surface area, surface charge carrier transfer rate, and electron−hole recombination rate. The lifetime of photogenerated electron−hole pairs will be increased by the formation of the phase junction, which is helpful to the photocatalytic process. Here, we have prepared $BiVO_4$ nanofibers with a phase junction structure by electrospinning versus calcination at different temperatures. Enhanced photocatalytic activity has been shown in the $BiVO_4$ nanofibers.

Up to now, several methods such as hydrothermal,[17] coprecipitation,[18] rapid microwave-assisted,[19] solid state reaction,[20] and templating fabrication[21] have been adopted for the preparation of $BiVO_4$. However, $BiVO_4$ prepared by these methods usually has a large crystal size, resulting in low surface area. In recent years, electrospun fibrous materials were found to be preferable for catalysts. The prepared ultrafine nanofibers present good photocatalytic activity due to their merits of large surface-to-volume ratios and recoverable character,[22] and, as compared to the powders, the nanofibers can be easily separated from the solution.[23] Moreover, phase

Received: February 12, 2015
Accepted: April 9, 2015
Published: April 9, 2015

DOI: 10.1021/acsami.5b01305
ACS Appl. Mater. Interfaces 2015, 7, 9638−9644

junction can be formed in the electrospun fibers by simply controlling the calcination temperature.[24]

In the present report, $BiVO_4$ nanofibers have been prepared by electrospinning method. Phase junction structure of scheelite tetragonal and monoclinic phases in the electrospun $BiVO_4$ nanofibers was obtained by the precisely controlled heat treatment. The photocatalyic activity of electrospun $BiVO_4$ nanofibers has been investigated using the degradation of rhodamine-B under visible light irradiation. The enhanced photocatalyst characters are discussed by density functional theory (DFT).

EXPERIMENTAL SECTION

$BiVO_4$ nanofibers were prepared by the following procedure. First, $Bi(NO_3)_3{\cdot}5H_2O$ was dissolved into HNO_3 solution. Citric acid then was added as a chelating agent, and after the homogeneous solution was obtained, aqueous ammonia was slowly added to the solution with stirring until a white precipitation came out and further dissolved. A second solution was prepared by dissolving the corresponding stoichiometric amount of NH_4VO_3 and also citric acid in distilled water. Afterward, the as-prepared solutions were mixed together. Ethanol and polyvinylpyrrolidone (PVP, MW = 1 300 000) then were added to the solution. The weight ratio of the starting materials was $Bi(NO_3)_3{\cdot}5H_2O$/PVP/ethanol/H_2O = 1/2.5/8/10. The concentrations of $Bi(NO_3)_3{\cdot}5H_2O$ and NH_4VO_3 are 0.103 mol/L. After complete dissolution, a clear transparent solution was obtained. The viscous solution was then put into a hypodermic syringe and electrospun with an applied high voltage of 20 kV at an electrode distance of about 20 cm; the grounded aluminum foil was used as a fiber collector. The as-spun nanofibers were then calcined at different temperatures, 350, 400, 450, 500, and 550 °C, for 1 h at a heating rate of 5 °C min^{-1}, respectively.

The photocatalytic activity of the prepared nanofibers was evaluated by the degradation of Rhodamine B (RhB) under visible light irradiation of a 300 W Xe lamp with a 400 nm cutoff filter. The incident photon flow was measured using a Digital Power & Energy meter (PM121D, Thorlabs Inc., Newton, NJ); the total optical power impinging on the solution was obtained with the known volume of solution irradiated as 109 ± 10 mW mL^{-1}. The nanofibers were dispersed in RhB solution (2.5×10^{-5} M, 10 mL) with a catalyst loading of 1g/L. The mixture was magnetically stirred in the dark for 2 h to obtain the adsorption/desorption equilibrium of RhB with the catalyst and then loaded in an open beaker with exposure to irradiation with continuous stirring at room temperature. At regular intervals of 10 min, UV−vis absorption spectra of the separated solution were measured. The absorption at 554 nm referring to the concentration of RhB was recorded as a function of irradiation time.

The morphology of the as-prepared products was characterized by scanning electron microscopy (SEM, JEOL JSM-6460LV, Tokyo, Japan). The phase of the $BiVO_4$ nanofibers was identified by X-ray diffraction (XRD, D/max-2550, Rigaku Co., Tokyo, Japan) and transmission electron microscopy (TEM, JEOL-2011, Tokyo, Japan). UV−visible (UV−vis) diffuse reflectance spectra (Shimadzu, UV3600) were recorded in the diffuse reflectance mode in the scan range of 300−800 nm. The X-ray photoelectron spectrum (XPS, PHI-5300 ESCA, PerkinElmer, Boston, MA) and the effective surface area determination (BET, QuadraSorb Station 2, Florida, USA) were also measured.

RESULTS AND DISCUSSION

Figure 1 demonstrates the SEM images of the as-spun $Bi(NO_3)_3/NH_4VO_3$/PVP fibers and the $BiVO_4$ nanofibers annealed at 450 °C. It is obvious that the surface of the as-spun fibers is smooth, while the calcined one becomes rough and the diameter has been reduced markedly.

The surface element compositions and chemical states of $BiVO_4$ nanofibers are revealed by XPS analysis (see Supporting Information Figure S1). The atomic concentration ratio of Bi/V is tested to be 1.03 ± 0.10. The phase structures of the $BiVO_4$ nanofibers are studied by XRD. Figure 2a shows the XRD patterns of the nanofibers annealed at different temperatures. The difference between the XRD patterns of $BiVO_4$ (s-m) and $BiVO_4$ (s-t) can be identified by the weak diffraction peak at 15° and splitting peaks at 2θ = 18.5°, 35°, and 46°.[15] It can be seen that $BiVO_4$ nanofibers calcined at 350 °C exhibit an incomplete tetragonal scheelite crystal structure (JCPDS no. 75-2481), while the diffraction patterns of the nanofibers calcined at 550 °C fit well with the scheelite-monoclinic phase (according to JCPDS no. 75-2480). As the temperature increases, the crystallinity of $BiVO_4$ nanofibers improves and the peak splitting has become clearer. Figure 2b shows the step-scanning XRD patterns from 34.5° to 36° of these $BiVO_4$ nanofibers. The 35° diffraction peak gradually splits into two. The phase gradually transforms from s-t $BiVO_4$ to s-m $BiVO_4$,[25]

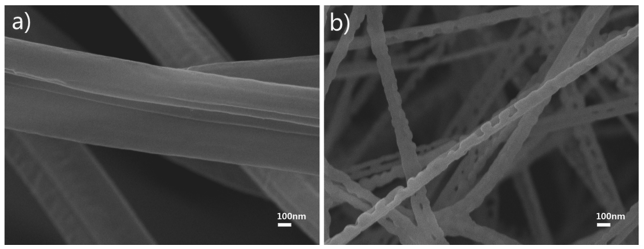

Figure 1. SEM images of (a) as-spun nanofibers and (b) the nanofibers annealed at 450 °C for 1 h in air.

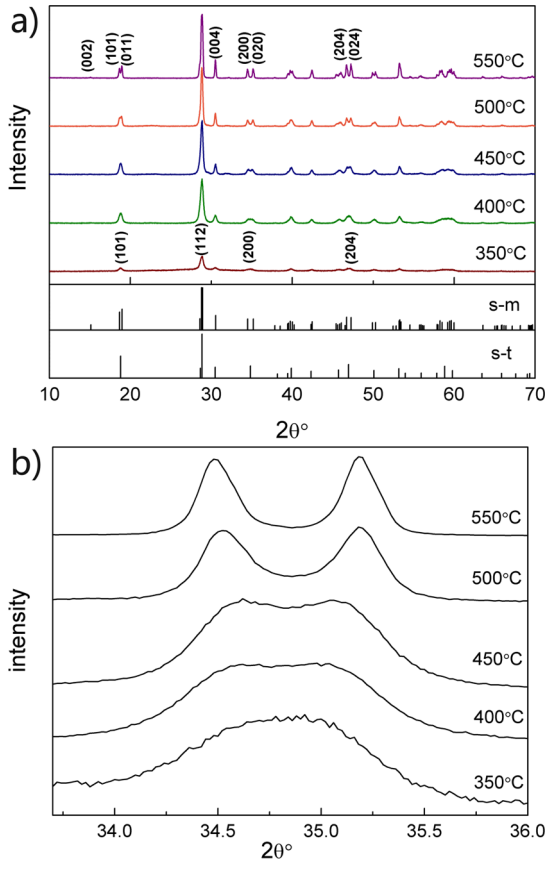

Figure 2. (a) XRD patterns of specimens calcined at different temperatures. (b) The step-scanning XRD of these $BiVO_4$ nanofibers.

DOI: 10.1021/acsami.5b01305
ACS Appl. Mater. Interfaces 2015, 7, 9638−9644

indicating that a phase junction is presented in the $BiVO_4$ nanofibers. A similar phase junction in semiconductors like TiO_2,[26] Ga_2O_3,[27] Bi_2O_3,[28] $BiPO_4$,[29] etc., could also be formed by adjusting the processing parameters.

Transmission electron microscopy (TEM) images of as-prepared $BiVO_4$ nanofibers at temperatures ranging from 400 to 550 °C are shown in Figure 3. The nanofiber calcined at 550 °C demonstrates a necklace structure. The inset of Figure 3d is the corresponding selected area electron diffraction (SAED) pattern, which matches well with the single crystalline structure of s-m $BiVO_4$, respectively. The HRTEM image of the $BiVO_4$ nanofibers calcined at 400 °C is shown in Figure 3a. The lattice fringes with d spacings of 0.293 and 0.308 nm are in good agreement with the (004) and (112) lattice planes of both scheelite tetragonal $BiVO_4$ (JCPDS no. 75-2481) and monoclinic $BiVO_4$ (JCPDS no. 75-2480). Figure 3b shows the HRTEM image of the $BiVO_4$ nanofibers calcined at 450 °C. The d spacing of 0.580 nm agrees well with the lattice spacings of (002) of s-m $BiVO_4$, while the d spacing of 0.470 nm matches well with (101) lattice planes of s-t $BiVO_4$, which confirms the existence of the phase junction in the nanofibers calcined at 450 °C. Further increasing the calcination temperature to 500 °C, $BiVO_4$ nanofibers possess the (101) and (011) lattice plane of s-m $BiVO_4$ (Figure 3c), which is in accord with the XRD result.

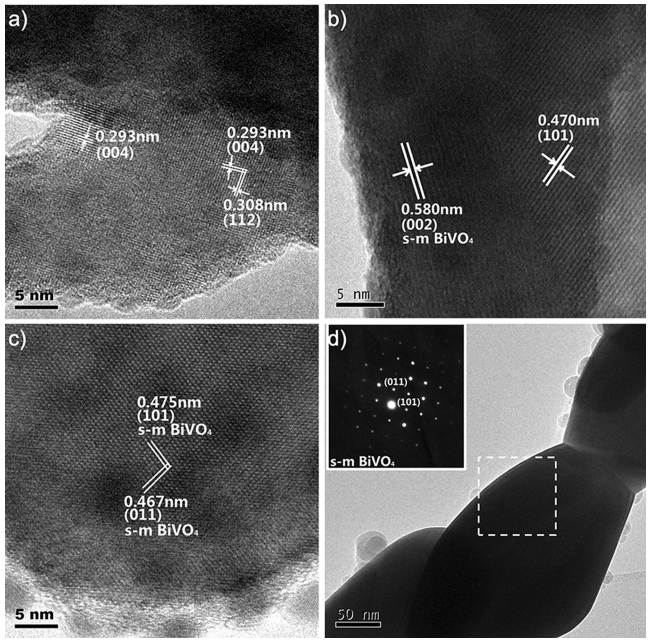

Figure 3. HRTEM images of the $BiVO_4$ nanofibers calcined at different temperatures: (a) 400 °C, (b) 450 °C, (c) 500 °C; and (d) SAED pattern of the $BiVO_4$ nanofibers calcined at 550 °C.

The photocatalytic activities of the nanofibers calcined at different temperature are evaluated by the degradation of RhB dye under visible light irradiation (λ = 400−750 nm). Catalyst loading of the nanofibers is 1 g/L. The total optical power impinging on the solution is 109 ± 10 mW mL^{-1}. The effective surface area of the nanofibers measured using the BET test is 18.97 ± 3.55 m^2/g. The normalized optical density change of RhB at 554 nm photocatalyzed by $BiVO_4$ nanofibers is plotted in Figure 4a as a function of time. When the phase junction is formed in $BiVO_4$ nanofibers, a remarkable enhancement in photocatalytic activity is observed. The optimal calcination temperature is 450 °C. RhB is almost completely degraded when irradiated under visible light for 40 min (Figure 4d), and the color of RhB solution turns clear (inset of Figure 4d). The RhB adsorbed on the sample surface is also removed (see FT-IR results, Supporting Information Figure S2). In comparison with the commercial TiO_2 powders (Degussa P-25), the photocatalytic activity of the $BiVO_4$ nanofibers is remarkably enhanced because TiO_2 can be activated only under UV radiation. It is known that the photodegradation of RhB can be considered as a pseudo-first-order reaction.[30,31] The degradation rate constant k can be calculated by the formula as follows:

$$C = C_0\, e^{-kt} \tag{1}$$

where t is the reaction time, C is the concentration of RhB after reacting for time t, and C_0 is the initial concentration, respectively. The relationship between the reaction rate constant k and the calcination temperature is shown in Figure 4b. The photocatalytic efficiency of the $BiVO_4$ nanofibers indicates a strong dependence on the calcination temperature. The nanofibers calcined at 450 °C show the highest catalytic activity with rate constant (k) of 0.10 min^{-1}, about 10 times the $BiVO_4$ nanofibers calcined at 350 °C (0.01 min^{-1}) for which the phase is scheelite tetragonal and 5 times higher than that calcined at 550 °C with the phase of pure scheelite monoclinic. The apparent quantum efficiency (AQE) is defined as follows:[32,33]

$$\mathrm{AQE} = \frac{\mathrm{d}[x]/\mathrm{d}t}{\mathrm{d}[h\nu]_{\mathrm{inc}}/\mathrm{d}t} = \frac{kC_0}{\mathrm{TOP}} \tag{2}$$

where $\mathrm{d}[x]/\mathrm{d}t$ is the initial rate of change of the concentration of the reactant; here, for the degradation of RhB, $\mathrm{d}[x]/\mathrm{d}t = kC_0$. $\mathrm{d}[h\nu]_{\mathrm{inc}}/\mathrm{d}t$ is the total optical power (TOP) impinging on the sample. As the catalyst loading of the nanofibers is 1g/L, the TOP impinging on the $BiVO_4$ nanofibers is 0.018 ± 0.002 mW/mL. On the basis of the experimental data, we estimated the apparent quantum efficiency (AQE) by using formula 2, and plotted them in Figure 4b. In the present research, AQE depends on the incident photons but not on the photons absorbed by the photocatalyst; the real quantum yield may be higher than the AQE obtained in this Article. It is indicated from Figure 4c that the photocatalytic activity of the nanofibers annealed at 450 °C is well stable in 8 time cycle tests, for which the RhB can still be almost completely degraded when irradiated under visible light in 40 min. The catalyst removed from the solution still demonstrates the three-dimensional open structure, although some nanofibers broke into small pieces during the dispersion and centrifugal separation process (Figure 4d). This character shows promising industrial application in eliminating the organic pollutants from wastewater.

It is important to investigate the mechanism of the enhanced photocatalytic activity of the phase junction structured electrospun $BiVO_4$ nanofibers. Here, we would like to discuss the photocatalytic process in detail by investigating the band structure of the $BiVO_4$ nanofibers. The UV−vis diffuse reflection spectra of the $BiVO_4$ nanofibers calcined at different temperatures were measured and are shown in Figure 5a. The nanofibers annealed at 350 °C have no obvious absorption edge because the crystallization is incomplete. The specimens calcined at 400−550 °C exhibit absorption in the visible light region, indicating the possibility for photocatalytic activity driven by visible light. The band gaps of the $BiVO_4$ nanofibers

DOI: 10.1021/acsami.5b01305
ACS Appl. Mater. Interfaces 2015, 7, 9638−9644

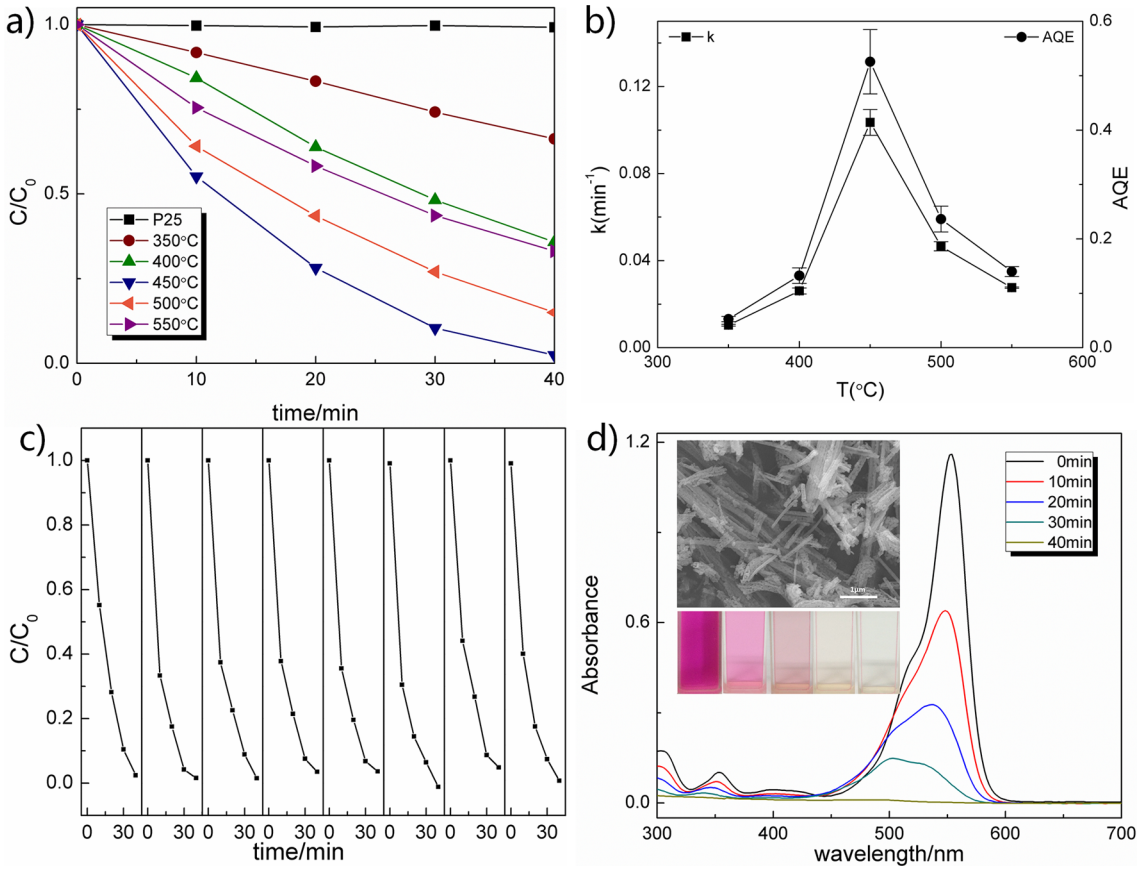

Figure 4. (a) Photodegradation of RhB by $BiVO_4$ nanofibers calcined at different temperatures; (b) degradation rate constants and apparent quantum efficiencies for $BiVO_4$ nanofibers; (c) the repeatability tests of the specimen calcined at 450 °C; (d) and the absorption spectrum of the RhB solution in the presence of $BiVO_4$ nanofibers. The inset illustrates photos for the RhB solutions photodegraded with different time and the SEM image of the specimen reclaimed after photocatalytic measurement.

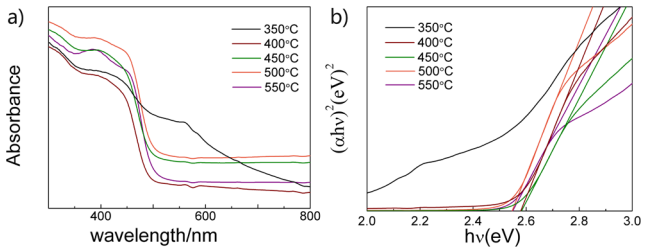

Figure 5. (a) UV−visible diffuse reflection spectra of the $BiVO_4$ fibers calcined at different temperatures, and (b) the corresponding plots of $(\alpha h\nu)^2$ versus photon energy ($h\nu$).

can be estimated on the basis of the UV−vis diffuse reflection spectra using the following formation:[34]

$$(\alpha h\nu)^2 = A(h\nu - E_g) \quad (3)$$

where α is the absorption coefficient, h is Planck's constant, ν is the incident light frequency, A is a constant, and E_g is the band gap, respectively. Therefore, the band gap of the $BiVO_4$ nanofibers can be estimated from the data shown in Figure 5b. The estimated E_g results of the nanofibers annealed at 400, 450, 500, and 550 °C are 2.58, 2.58, 2.55, and 2.55 eV, respectively. It is found that the band gap of $BiVO_4$ nanofibers is a function of annealing temperature.

The band structure of the semiconductor materials could also be predicted using first principle calculation. In the present study, we calculated the band structure of the phase junction structure in electrospun $BiVO_4$ nanofibers using first principle calculation. The crystal structure of $BiVO_4$ (s-m) is similar to that of $BiVO_4$ (s-t) due to the same scheelite structure. The distinct feature of the two $BiVO_4$ phases is that their basic structural unit is constructed by VO_4 tetrahedra and BiO_8 dodecahedron. The difference between s-m and s-t $BiVO_4$ is only the oxygen position (see Supporting Information Figure S3). This depends on the changed lattice parameters at low or high temperature. The partial densities of states (DOS) of s-m/s-t $BiVO_4$ phases are shown in Figure 6.

The lower valence bands have little effect on photocatalytic properties. The valence band (VB) mainly consists of O 2p and minor Bi 6s. The conduction band (CB) strongly hybridized with V 3d states, O 2p states, and Bi 6p states. In CB, V 3d states are split into two parts, which contain $3d_{x2-y2}$ and $3d_{z2}$ states, and $3d_{xy}$, $3d_{yz}$, and $3d_{xz}$ states. The photocatalytic activity should be enhanced by the tetrahedral crystal field effect.[35] In our first principle calculation, we have used the advanced hybrid functional HSE06[36] to describe the exchange-correlation potential avoiding the self-interaction effects between electrons to make the calculated results more accurate. The calculated results (shown in Figure 6) indicate that the band gaps of s-m and s-t phase $BiVO_4$ are 2.5 and 3.1 eV, respectively. Some reported calculations and experimental results are close to us.[37−39] Our estimated value of band gap in the electrospun $BiVO_4$ nanofibers by UV−vis diffuse reflection spectra measurement is 2.55−2.58 eV depending on the calcination temperature, which is between the calculated values of s-m

DOI: 10.1021/acsami.5b01305
ACS Appl. Mater. Interfaces 2015, 7, 9638−9644

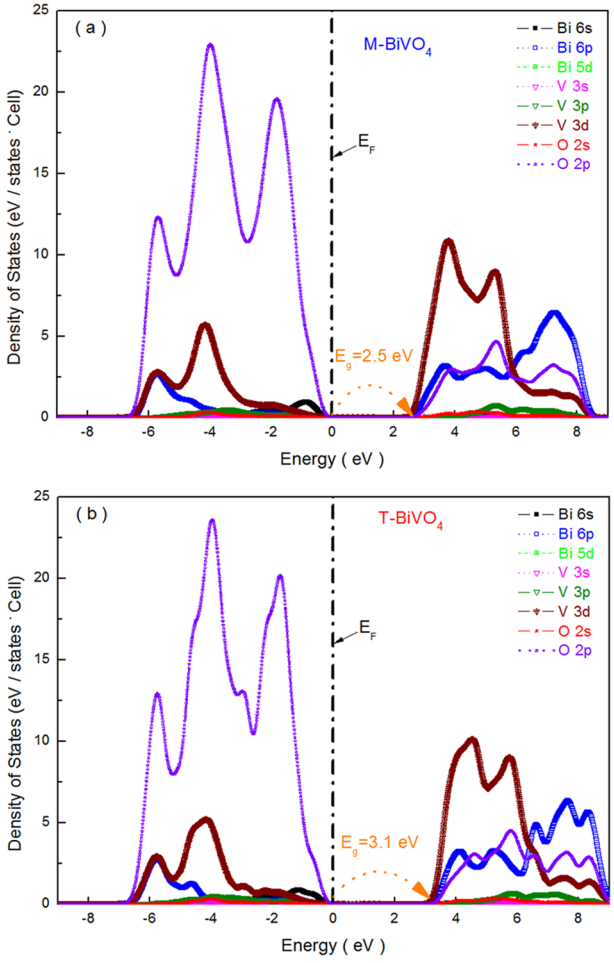

Figure 6. Electron densities of states of (a) s-m $BiVO_4$ (E_g, 2.5 eV) and (b) s-t $BiVO_4$ (E_g, 3.1 eV). The dashed line is the Fermi level.

phase and s-t phase $BiVO_4$, indicating that the phase junction structure of s-m/s-t phases exists in the electrospun $BiVO_4$ nanofibers.

The mechanism of phase-dependent photocatalytic activity in phase junction $BiVO_4$ nanofibers is schematically shown in Figure 7. In our study, the contents of scheelite tetragonal phase in the phase junction electrospun $BiVO_4$ nanofibers are different at various annealing temperatures. As schematized in Figure 7, when the catalysts are illuminated by visible light with

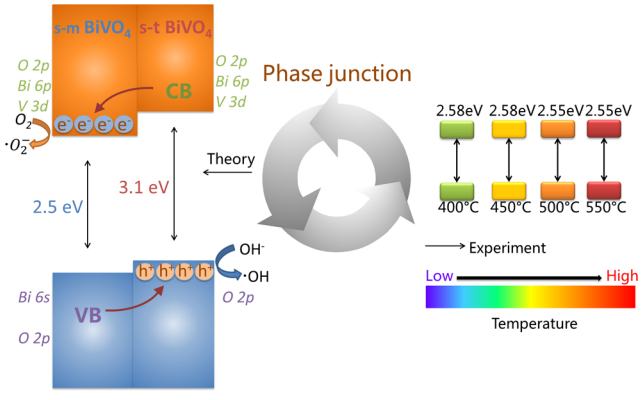

Figure 7. Schematic illustrations of the band structure related photocatalytic mechanism for the s-m/s-t $BiVO_4$ phase junction.

photon energy higher than the band gap of $BiVO_4$, electrons in the valence band can be excited to the CB with the generation of the same amount of holes. In the phase junction structure of the $BiVO_4$ nanofibers, the electrons will transfer from s-t $BiVO_4$ to the scheelite monoclinic electron-trapping site. The lifetime of photogenerated electron−hole pairs will be increased. The photoinduced holes are apt to react with surface-bound H_2O or OH^- to produce the hydroxyl radical species ($^{\bullet}OH$), which is an extremely strong oxidant for the mineralization of organic chemicals. The RhB molecules can be oxidized into inorganic molecules (e.g., CO_2, H_2O) or ions (e.g., NO_3^-, and Cl^-).[40]

On the other hand, we can also discuss the mechanism of photocatalytic activity in phase junction structured $BiVO_4$ nanofibers from the aspects of the optical character of semiconductor materials. For optical properties, the linear response of the electron gas can be described by the complex dielectric function:

$$\varepsilon(\omega) = \varepsilon_1(\omega) + i\varepsilon_2(\omega) \tag{4}$$

$$\varepsilon_1(\omega) = 1 + \frac{2}{\pi} p \int_0^{\infty} \frac{\omega' \varepsilon_2(\omega')\, \mathrm{d}\omega'}{\omega'^2 - \omega^2} \tag{5}$$

$$\varepsilon_2(\omega) = \left(\frac{4\pi^2 e^2}{m^2 \omega^2}\right) \sum_{i,j} \int \langle i|M|j\rangle^2 f_i (1 - f_i)\, \delta(E_f - E_i - \omega)\, \mathrm{d}^3k \tag{6}$$

The dielectric function depends on the electronic band structure of a crystal, and it also strongly depends on the photon frequency of compounds. The dielectric function is proportional to the integrality of the dipole interband transition probability as shown in Figure 8a.

The constraint of selection rule for the electronic interband transition is that the dielectric function reflects the characteristics of the band structure and the PDOS near the Fermi level. On the basis of the analysis of electronic structure in s-m/s-t $BiVO_4$, it is clear that the peaks of $\varepsilon_2(\omega)$ near the absorption edge mainly originated from the electron transition from O 2p occupied states to V 3d unoccupied states. The other peaks are contributed by the electron transition from O 2p occupied states to Bi 6p unoccupied states. While comparing the monoclinic and tetragonal phases, both the real (Re) and the imaginary (Im) parts of the tetragonal phase are higher than those of the monoclinic phase in the long wavelength of photon. The absorption of s-m/s-t $BiVO_4$ is shown in Figure 8b. It can be seen the monoclinic phase has a good absorption in the "green" light (wavelength from 480 to 620 nm). Yet the tetragonal phase has a larger band gap, which requires the higher energy of photon (violet light) for the transition. Additionally, it has higher absorption coefficient than the monoclinic phase in the longer wavelength of photons. It helps the phase junction to get more energy to increase the photocatalyst activity. This is in agreement with the experiments by UV−vis reflection. According to Kweon's results,[41] the theoretical evidence confirms the phase dependence of hole localization and transport in bismuth vanadate for photocatalyst properties.

CONCLUSION

Tetragonal sheelite (s-t) and monoclinic sheelite (s-m) phases $BiVO_4$ nanofibers with a phase junction have been successfully prepared via a simple electrospinning process and controlled

DOI: 10.1021/acsami.5b01305
ACS Appl. Mater. Interfaces 2015, 7, 9638−9644

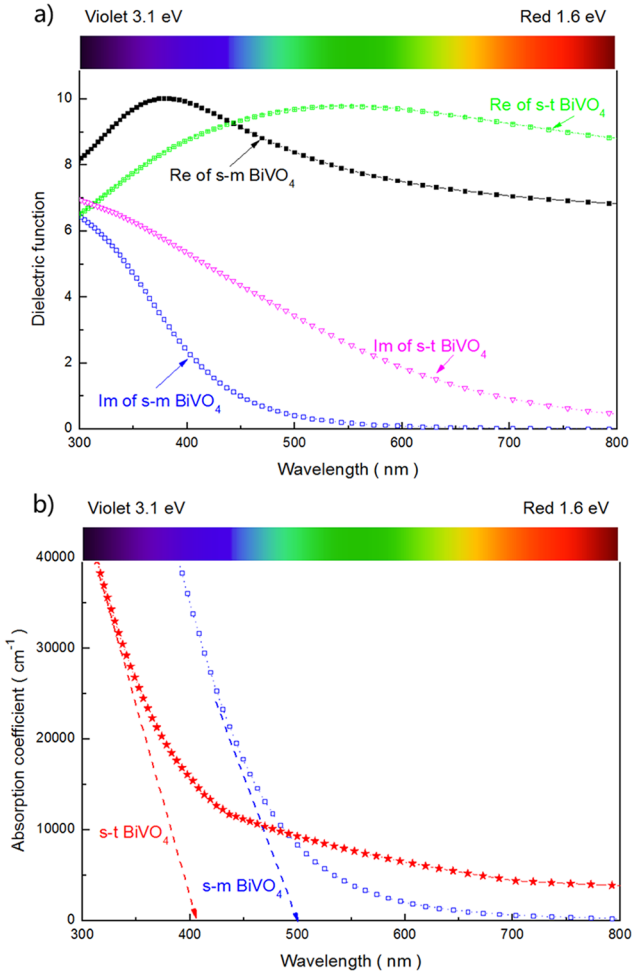

Figure 8. (a) Dielectric functions as a function of photon energy of s-m/s-t $BiVO_4$ in theory; (b) absorption coefficients as a function of photon energy of s-m/s-t $BiVO_4$, with the absorption edge of s-m/s-t $BiVO_4$ phases corresponding to the 410 and 500 nm photon wavelength, respectively.

calcination. The obtained nanofibers show an enhanced photocatalytic activity in the decomposition of RhB under visible light irradiation. Structure, phase analysis, and band structure calculation results reveal that the enhanced photocatalytic activity is attributed to the phase junction structure of the (s-t) and (s-m) phases in electrospun $BiVO_4$ nanofibers. The results in the current work may be beneficial to the future study of exploring the visible light-driven photocatalysis materials.

■ ASSOCIATED CONTENT

Supporting Information

Characterization details. This material is available free of charge via the Internet at http://pubs.acs.org.

■ AUTHOR INFORMATION

Corresponding Author

*E-mail: panw@mail.tsinghua.edu.cn.

Notes

The authors declare no competing financial interest.

■ ACKNOWLEDGMENTS

This study was supported by the Natural Science Foundation of China (Grant no. 51323001).

■ REFERENCES

(1) Ohtani, B. Preparing Articles on Photocatalysis - Beyond the Illusions, Misconceptions, and Speculation. *Chem. Lett.* **2008**, *37*, 216−229.
(2) Li, H. P.; Zhang, W.; Pan, W. Enhanced Photocatalytic Activity of Electrospun TiO_2 Nanofibers with Optimal Anatase/Rutile Ratio. *J. Am. Ceram. Soc.* **2011**, *94*, 3184−3187.
(3) Asahi, R.; Morikawa, T.; Ohwaki, T.; Aoke, K.; Taga, Y. Visible-light Photocatalysis in Nitrogen-Doped Titanium Oxides. *Science* **2001**, *293*, 269−271.
(4) Chen, X. B.; Liu, L.; Yu, P. Y.; Mao, S. S. Increasing Solar Absorption for Photocatalysis with Black Hydrogenated Titanium Dioxide Nanocrystals. *Science* **2011**, *331*, 746−750.
(5) Chen, X. B.; Lou, Y. B.; Samia, A. C. S.; Burda, C.; Gole, J. L. Formation of Oxynitride as the Photocatalytic Enhancing site in Nitrogen-Doped Titania Nanocatalysts: Comparison to a Commercial Nanopowder. *Adv. Funct. Mater.* **2005**, *15*, 41−49.
(6) Khan, R.; Kim, T. Preparation and Application of Visible-Light-Responsive Ni-Doped and SnO_2-Coupled TiO_2 Nanocomposite Photocatalysts. *J. Hazard. Mater.* **2009**, *163*, 1179−1184.
(7) Kudo, A.; Omori, K.; Kato, H. A Novel Aqueous Process for Preparation of Crystal Form-Controlled and Highly Crystalline $BiVO_4$ Powder from Layered Vanadates at Room Temperature and its Photocatalytic and Photophysical Properties. *J. Am. Chem. Soc.* **1999**, *121*, 11459−11467.
(8) Shang, M.; Wang, W.; Ren, J.; Sun, S.; Wang, L.; Zhang, L. A Practical Visible-Light-Driven Bi_2WO_6 Nanofibrous Mat Prepared by Electrospinning. *J. Mater. Chem.* **2009**, *19*, 6213−6218.
(9) Kato, H.; Kobayashi, H.; Kudo, A. Role of Ag^+ in the Band Structures and Photocatalytic Properties of $AgMO_3$ (M: Ta and Nb) with the Perovskite Structure. *J. Phys. Chem. B* **2002**, *106*, 12441−12447.
(10) Kudo, A.; Kato, H.; Tsuji, I. Strategies for the Development of Visible-Light-Driven Photocatalysts for Water Splitting. *Chem. Lett.* **2004**, *33*, 1534−1539.
(11) Park, Y.; McDonald, K. J.; Choi, K. S. Progress in Bismuth Vanadate Photoanodes for Use in Solar Water Oxidation. *Chem. Soc. Rev.* **2013**, *42*, 2321−2337.
(12) Meng, X.; Zhang, L.; Dai, H. X.; Zhao, Z. X.; Zhang, R. Z.; Liu, Y. X. Surfactant-Assisted Hydrothermal Fabrication and Visible-Light-Driven Photocatalytic Degradation of Methylene Blue over Multiple Morphological $BiVO_4$ Single-Crystallites. *Mater. Chem. Phys.* **2011**, *125*, 59−65.
(13) Lim, A. R.; Choh, S. H.; Jang, M. S. Prominent Ferroelastic Domain Walls in $BiVO_4$ Crystal. *J. Phys.: Condens. Matter.* **1995**, *7*, 7309−7323.
(14) Hirota, K.; Komatsu, G.; Yamashita, M.; Takemura, H.; Yamaguchi, O. Formation, Characterization and Sintering of Alkoxy-Derived Bismuth Vanadate. *Mater. Res. Bull.* **1992**, *27*, 823−830.
(15) Tokunaga, S.; Kato, H.; Kuto, A. Selective Preparation of Monoclinic and Tetragonal $BiVO_4$ with Scheelite Structure and Their Photocatalytic Properties. *Chem. Mater.* **2001**, *13*, 4624−4628.
(16) Kohtani, S.; Koshiko, M.; Kudo, A.; Tokumura, K.; Ishigaki, Y.; Toriba, A.; Hayakawa, K.; Nakagaki, R. Photodegradation of 4-Alkylphenols Using $BiVO_4$ Photocatalyst under Irradiation with Visible Light from a Solar Simulator. *Appl. Catal., B* **2003**, *46*, 573−586.
(17) Yu, J. Q.; Kudo, A. Effects of Structural Variation on the Photocatalytic Performance of Hydrothermally Synthesized $BiVO_4$. *Adv. Funct. Mater.* **2006**, *16*, 2163−2169.
(18) Yu, J. Q.; Zhang, Y.; Kudo, A. Synthesis and Photocatalytic Performances of $BiVO_4$ by Ammonia Co-precipitation Process. *J. Solid State Chem.* **2009**, *182*, 223−228.
(19) Zhang, H. M.; Liu, J. B.; Wang, H.; Zhang, W. X.; Yan, H. Rapid Microwave-Assisted Synthesis of Phase Controlled $BiVO_4$ Nanocryst-

DOI: 10.1021/acsami.5b01305
ACS Appl. Mater. Interfaces 2015, 7, 9638−9644

als and Research on Photocatalytic Properties under Visible Light Irradiation. *J. Nanopart. Res.* **2008**, *10*, 767−774.
(20) Gotić, M.; Musić, S.; Ivanda, M.; Soufek, M.; Popović, S. Synthesis and Characterisation of Bismuth (III) Vanadate. *J. Mol. Struct.* **2005**, *744*, 535−540.
(21) Liu, Y. X.; Dai, H. X.; Deng, J. G.; Zhang, L.; Au, C. T. Three-dimensional Ordered Macroporous Bismuth Vanadates: PMMA-templating Fabrication and Excellent Visible light-driven Photocatalytic Performance for Phenol Degradation. *Nanoscale* **2012**, *4*, 2317−2325.
(22) Wu, H.; Pan, W.; Lin, D. D.; Li, H. P. Electrospinning of Ceramic Nanofibers: Fabrication, Assembly and Applications. *J. Adv. Ceram.* **2012**, *1*, 2−23.
(23) Lin, D. D.; Wu, H.; Zhang, R.; Pan, W. Enhanced Photocatalysis of Electrospun Ag-ZnO Heterostructured Nanofibers. *Chem. Mater.* **2009**, *21*, 3479−3484.
(24) Ou, G.; Liu, W.; Yao, L.; Wu, H.; Pan, W. High Conductivity of $La_2Zr_2O_7$ Nanofibers by Phase Control. *J. Mater. Chem. A* **2014**, *2*, 1855−1861.
(25) Kho, Y. K.; Teoh, W. Y.; Iwase, A.; Madler, L.; Kudo, A.; Amal, R. Flame Preparation of Visible-Light-Responsive $BiVO_4$ Oxygen Evolution Photocatalysts with Subsequent Activation via Aqueous Route. *ACS Appl. Mater. Interfaces* **2011**, *3*, 1997−2004.
(26) Zhang, J.; Xu, Q.; Feng, Z.; Li, M.; Li, C. Importance of the Relationship between Surface Phases and Photocatalytic Activity of TiO_2. *Angew. Chem., Int. Ed.* **2008**, *47*, 1766−1769.
(27) Wang, X.; Xu, Q.; Li, M.; Shen, S.; Wang, X.; Wang, Y.; Feng, Z.; Shi, J.; Han, H.; Li, C. Photocatalytic Overall Water Splitting Promoted by an Alpha-Beta Phase Junction on Ga_2O_3. *Angew. Chem., Int. Ed.* **2012**, *51*, 13089−13092.
(28) Hou, J.; Yang, C.; Wang, Z.; Zhou, W.; Jiao, S.; Zhu, H. In situ Synthesis of Alpha-Beta Phase Heterojunction on Bi_2O_3 Nanowires with Exceptional Visible-Light Photocatalytic Performance. *Appl. Catal., B* **2013**, *142*, 504−511.
(29) Zhu, Y.; Liu, Y.; Lv, Y.; Ling, Q.; Liu, D.; Zhu, Y. Enhancement of Photocatalytic Activity for $BiPO_4$ via Phase Junction. *J. Mater. Chem. A* **2014**, *2*, 13041−13048.
(30) Liu, Z. Y.; Sun, D. D.; Guo, P.; Leckie, J. O. An Efficient Bicomponent TiO_2/SnO_2 Nanofiber Photocatalyst Fabricated by Electrospinning with a Side-by-Side Dual Spinneret Method. *Nano Lett.* **2007**, *7*, 1081−1085.
(31) Wan, Q.; Wang, T. H.; Zhao, J. C. Enhanced Photocatalytic Activity of ZnO Nanotetrapods. *Appl. Phys. Lett.* **2005**, *87*, 083105−083107.
(32) Salinaro, A.; Emeline, A. V.; Zhao, J.; Hidaka, H.; Ryabchuk, V. K.; Serpone, N. Terminology, Relative Photonic Efficiencies and Quantum Yields in Heterogeneous Photocatalysis. Part II: Experimental Determination of Quantum Yields. *Pure Appl. Chem.* **1999**, *71*, 321−335.
(33) Wachs, I. E.; Phivilay, S. P.; Roberts, C. A. Reporting of Reactivity for Heterogeneous Photocatalysis. *ACS Catal.* **2013**, *3*, 2606−2611.
(34) Butler, M. A. Photoelectrolysis and Physical Properties of the Semiconducting Electrode WO_2. *J. Appl. Phys.* **1977**, *48*, 1914−1920.
(35) Zhao, Z.; Li, Z.; Zou, Z. Electronic Structure and Optical Properties of Monoclinic Clinobisvanite $BiVO_4$. *Phys. Chem. Chem. Phys.* **2011**, *13*, 4746−4753.
(36) Heyd, J.; Scuseria, G. E. Hybrid Functionals Based on a Screened Coulomb Potential. *J. Chem. Phys.* **2003**, *118*, 8207−8215.
(37) Li, G.; Bai, Y.; Zhang, W. F. Difference in Valence Band Top of $BiVO_4$ with Different Crystal Structure. *Mater. Chem. Phys.* **2012**, *136*, 930−934.
(38) Yin, W.; Wei, S.; Al-Jassim, M. M.; Turner, J.; Yan, Y. Doping Properties of Monoclinic $BiVO_4$ Studied by First-Principles Density-Functional Theory. *Phys. Rev. B* **2011**, *83*, 155102.
(39) Walsh, A.; Yan, Y.; Huda, M. N.; Al-Jassim, M. M.; Wei, S. Band Edge Electronic Structure of $BiVO_4$: Elucidating the Role of the Bi s and V d Orbitals. *Chem. Mater.* **2009**, *21*, 547−551.
(40) Wang, Y.; Dai, H. X.; Deng, J. G.; Liu, Y. X.; Arandiyan, H.; Li, X. W.; Gao, B. Z.; Xie, S. H. 3DOM InVO4-Supported Chromia with Good Performance for the Visible-Light-Driven Photodegradation of Rhodamine B. *Solid State Sci.* **2013**, *24*, 62−70.
(41) Kweon, K. E.; Hwang, G. S. Structural Phase-Dependent Hole Localization and Transport in Bismuth Vanadate. *Phys. Rev. B* **2013**, *87*, 205202.

DOI: 10.1021/acsami.5b01305
ACS Appl. Mater. Interfaces 2015, 7, 9638−9644